Accelerated Publications

The Immunosuppressive Agent Mizoribine Monophosphate Forms a Transition State Analogue Complex with Inosine Monophosphate Dehydrogenase†

Lu Gan,‡ Mohammad R. Seyedsayamdost,‡,§ Satoshi Shuto,|| Akira Matsuda,|| Gregory A. Petsko,‡,⊥ and Lizbeth Hedstrom*,‡

Departments of Biochemistry and Chemistry and the Rosenstiel Basic Medical Sciences Research Center, Brandeis University, Waltham, Massachusetts 02454, and Graduate School of Pharmaceutical Sciences, Hokkaido University, Sapporo 060-0812, Japan

Received November 8, 2002; Revised Manuscript Received December 8, 2002

ABSTRACT: Mizoribine monophosphate (MZP) is the active metabolite of the immunosuppressive agent mizoribine and a potent inhibitor of IMP dehydrogenase (IMPDH). This enzyme catalyzes the oxidation of IMP to XMP with the concomitant reduction of NAD via a covalent intermediate at Cys319 (E-XMP*). Surprisingly, mutational analysis indicates that MZP is a transition state analogue although its structure does not resemble that of the expected transition state. Here we report the X-ray crystal structure of the E·MZP complex at 2.0 Å resolution that reveals a transition state-like structure and solves the mechanistic puzzle of the IMPDH reaction. The protein assumes a new conformation where a flap folds into the NAD site and MZP, Cys319, and a water molecule are arranged in a geometry resembling the transition state. The water appears to be activated by interactions with a conserved Arg418−Tyr419 dyad. Mutagenesis experiments confirm that this new closed conformation is required for the hydrolysis of E-XMP*, but not for the reduction of NAD. The closed conformation provides a structural explanation for the differences in drug selectivity and catalytic efficiency of IMPDH isozymes.

Inosine 5′-monophosphate dehydrogenase (IMPDH)[1] controls a critical junction in the metabolism of nucleic acid precursors: the conversion of IMP to XMP with reduction of NAD is the rate-limiting step in de novo guanine nucleotide biosynthesis (*1*). Proliferation is strongly linked to the size of the guanine nucleotide pool, which makes IMPDH an attractive target for chemotherapy, and inhibitors of IMPDH are used as immunosuppressive (*2*), anticancer (*3*), and antiviral agents (*4*, *5*). MZP is the active metabolite of the immunosuppressive drug mizoribine and a potent inhibitor of IMPDH (K_i = 3.9 and 0.5 nM for human type 2 and *Escherichia coli* IMPDHs, respectively) (*6*−*8*) (Figure 1). As generally observed for transition state analogue inhibitors (*9*), the affinity of MZP decreases in parallel with activity for a series of IMPDH mutants (*8*). This behavior is surprising because MZP does not have the structure expected for the transition state of the IMPDH reaction (Figure 1).

The IMPDH reaction involves two very different chemical transformations: hydride transfer and hydrolysis (Figure 1) (*10*). The active site Cys attacks the 2 position of IMP, and hydride is transferred to NAD, forming the covalent E-XMP* intermediate. NADH dissociates, water attacks the 2 position and E-XMP* hydrolyzes (*11*). The hydrolysis of E-XMP* is rate-limiting and would be expected to proceed via a tetrahedral intermediate/transition state analogous to the hydrolysis of acylenzyme intermediates in protease reactions (Figure 1). MZP clearly does not mimic this tetrahedral geometry. In addition, enzymatic hydrolysis reactions generally require a mechanism to activate water; despite extensive investigation, this mechanism has not yet been identified in the IMPDH.

The active site of IMPDH is characterized by disorder that suggests a dynamic structure is required for catalysis. The enzyme is a homotetramer; each monomer contains an α/β barrel catalytic domain and a ∼100 residue subdomain of unknown function (*12*, *13*). Removal of the subdomain has no effect on IMPDH activity (*14*, *15*). The active site Cys319 is found on a small mobile loop that can assume various conformations or be disordered depending on the ligand present (the "active site loop", residues 314−324 in *T. foetus* IMPDH numbering) (*16*). A second mobile loop (the "flap",

† Supported by NIH GM54403 (L.H.), NIH GM 32415 (G.A.P.), and a grant from the Markey Charitable Trust to Brandeis University.

* To whom correspondence should be addressed. Telephone: (781)-736-2333. Fax: (781)-736-2349. E-mail: hedstrom@brandeis.edu.

‡ Department of Biochemistry, Brandeis University.

§ Present address: Department of Chemistry, Massachusetts Institute of Technology, Cambridge, MA 02139.

|| Hokkaido University.

⊥ Department of Chemistry and the Rosenstiel Basic Medical Sciences Research Center, Brandeis University.

[1] Abbreviations: IMPDH, inosine 5′-monophosphate dehydrogenase; MZP, mizoribine monophosphate; IMP, inosine 5′-monophosphate; NAD, nicotinamide adenine dinucleotide; NADH, reduced nicotinamide adenine dinucleotide; XMP, xanthosine 5′-monophosphate; ADP, adenosine-5′-diphosphate; MPA, mycophenolic acid; β-Me-TAD, β-methylene thiazole-4-carboxamide adenine dinucleotide; tiazofurin, 2-β-D-ribofuranosylthiazole-4-carboxamide; DTT, dithiothreitol; SAD, selenazole-4-carboxamide adenine dinucleotide.

10.1021/bi0271401 CCC: $25.00
Published on Web 01/04/2003

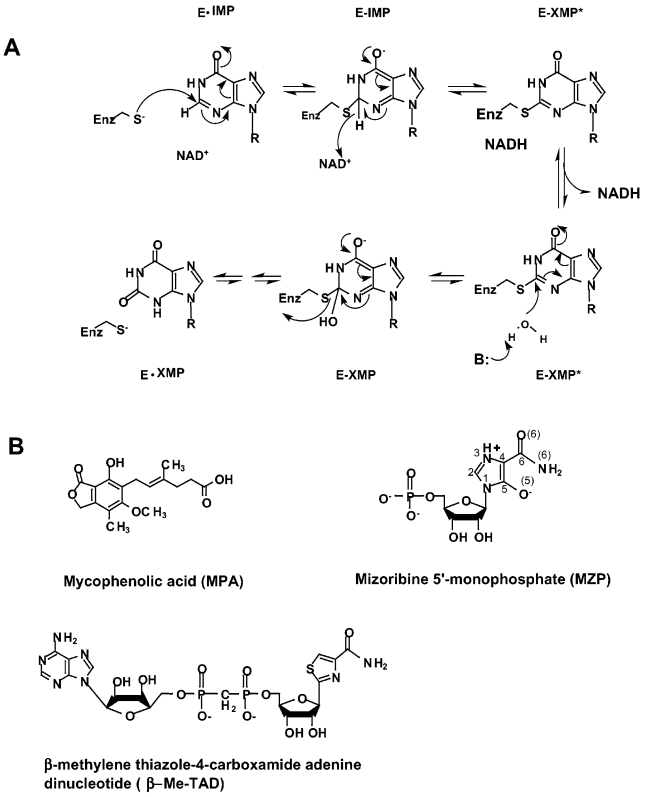

FIGURE 1: The mechanism of IMPDH reaction and the structures of IMPDH inhibitors. (A) The chemical mechanism of IMPDH reaction. The reaction is initiated by the attack of the catalytic Cys on 2 position of IMP. A hydride is transferred to NAD to form NADH and the covalent intermediate E-XMP*. NADH release precedes the hydrolysis of E-XMP*. E-XMP* is hydrolyzed, generating XMP and the free enzyme. A catalytic base is expected to activate the water to facilitate the hydrolysis. (B) Structures of IMPDH inhibitors, mizoribine 5-monophosphate (MZP), mycophenolic acid (MPA), and β-methylene thiazole-4-carboxamide adenine dinucleotide (β-Me-TAD). The atomic numbering of the base moiety of MZP is adopted as previously reported (*37*).

residues 407−433) also displays varying amounts of disorder depending on the ligand present (*12*, *13*, *15*, *17*−*19*). The proximal portion of the flap forms a lid over the active site and becomes ordered when ligands bind in the IMP site and the nicotinamide subsite. However, the distal portion of the flap (residues 417−430) is disordered, and the adenosine subsite is exposed to solvent in all of the published IMPDH structures.

IMPDH is activated by K^+, and this process may also be dynamic (*15*, *20*−*22*)**.** The active site loop forms part of a K^+ binding site (site 1) (*12*, *23*). However, this K^+ has only been observed in the E-XMP*·MPA complex of Chinese hamster IMPDH (*12*). The conformation of the active site loop is not compatible with K^+ binding in other IMPDH complexes (*13*, *17*−*19*), including the E·IMP·β-Me-TAD complex of *T. foetus* IMPDH, which should mimic the ternary complex prior to hydride transfer (*15*). These observations suggest that site 1 is created when E-XMP* forms, so that K^+ binding stabilizes E-XMP*. A second K^+ site is observed in the vicinity of the NAD site in *T. foetus* IMPDH and appears to be present throughout the catalytic cycle (*15*).

We report here the 2.0 Å resolution crystal structure[2] of the catalytic domain of *Tritrichomonas foetus* IMPDH in complex with MZP. This structure confirms the transition state analogy of MZP, reveals a novel mechanism for activating water, and describes a dynamic conformational change that controls drug selectivity and catalysis.

Table 1: Statistics for Data Collection and Refinement

Data Collection	
temperature	100 K
space group	$P2_12_12_1$
unit cell (Å)	
a	96.75
b	112.57
c	159.76
$\alpha = \beta = \gamma$ (deg)	90.00
resolution (Å)	2.0
total no. of reflections	1775920
no. of unique reflections	113342 [$I/\sigma(I) > 0$]
overall $\langle I/\sigma(I)\rangle$	>22
completeness of data (%; overall/ 2.00−2.07 Å)	99.1/99.9
R-merge[a] (%; overall/ 2.00−2.07 Å)	6.9/18.1
Refinement	
resolution range (Å)	8.0−2.0
reflections used (working/free)	102001/11341
temperature factor model	restrained group
R-factor[b]/*R*-free (%)	19.6/22.2
model used in refinement (tetramer)	
total non-hydrogen atoms in protein	11084
no. of waters	970
no. of Mizoribine-5′-monophosphate	4
no. of potassium ion	8
no. of Tris	6
rms deviations from ideal geometry[c]	
bond length (Å)	0.006
bond angles (deg)	1.28
dihedral angles (deg)	22.6
improper angles (deg)	0.76

[a] *R*-merge = $\Sigma|I_{obs} - I_{avg}|/\Sigma I_{avg}$, over all symmetry-related observations. [b] *R*-factor = $\Sigma|F_{obs} - F_{avg}|/\Sigma F_{avg}$, over all reflections. [c] Engh and Huber parameters were used in refinement.

EXPERIMENTAL PROCEDURES

Materials. The phosphorylation of mizoribine by usual methods was unsuccessful due to its unusual zwitterionic structure of the base moiety. Therefore, MZP was synthesized via a novel photochemical imidazole ring-cleavage reaction as the key step (*24*).

Crystallization, Data Collection, and Structure Determination. The catalytic domain of *T. foetus* IMPDH was expressed and purified as previously described (*15*). Crystals were grown at room temperature using the hanging drop vapor-diffusion method. Crystals were obtained by mixing equal volumes of the protein solution [2.0 mg ml^{-1} IMPDH catalytic domain, 20 mM Tris-HCl (pH 7.5), 5% glycerol, 0.6 mM MZP, 1 mM DTT] and reservoir solution [10% PEG 10,000, 100 mM MES (pH 6.25), 120 mM KCl, 20% glycerol, 1 mM DTT]. Data were collected from a single crystal at 100 K on the CCD detector on beamline 14 BMC at Advanced Photon Source (Argonne National Laboratory, Argonne, IL). X-ray wavelength was 1.00 Å. The data were processed and scaled with DENZO and SCALEPACK (*25*). The crystal belongs to the space group $P2_12_12_1$ (a = 96.75 Å, b = 112.57 Å, c = 159.76 Å), and the asymmetric unit

[2] The crystal structure described in this paper has been deposited in Protein Data Bank with accession code 1MWF.

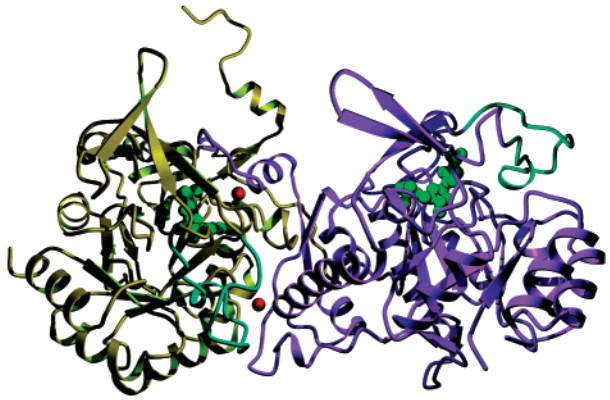

FIGURE 2: The structure of the E·MZP complex. Two monomers of the catalytic domain tetramer of *T. foetus* IMPDH are shown in complex with MZP. Monomer A is yellow, monomer B is magenta, the distal flap (residues 413−431) is cyan, MZP is green, and the two potassium ions are red. The figures were generated with Molscript (*38*) and rendered with POV-Ray.

contains a tetramer. The structure was solved by molecular replacement with AmoRe software in CCP4 (*26*) using structure of the E·IMP·β-Me-TAD complex of the catalytic domain of *T. foetus* IMPDH as the search model (PDB accession code 1LRT) (*15*). The active site flap is disordered in the search model. Rigid-body refinement was performed directly with the tetramer search model and the reduced data, generating a solution with an initial *R*-factor of 45.4%.

Structure Refinement. Subsequent structural refinement and model-building were performed using program package CNS 1.0 (*27*) and O 7.0 (*28*). After simulated annealing refinement with NCS restraints, the $2F_o-F_c$ density map and F_o-F_c difference map were generated. Clear and continuous electron density was observed in the area of the active site loop, active site flap and C-terminus of the enzyme in difference map. Clear electron density was also observed in the IMP site corresponding to MZP. MZP and the missing residues were gradually added to fit the density in the subsequent conjugate-gradient minimization and individual *B*-factor refinement. Water molecules were added into the model at the late stage of the refinement. Two water molecules at subunit interfaces were finally modeled as potassium ions on the basis of their strong density and geometry of the coordination to the protein ligands. The final model contains 362 of 376 residues, one molecule of MZP, and two molecules of potassium ion per monomer. The entire tetramer structure also contains 970 water and 6 Tris molecules. Residues 100−227−228−229−230 in the linker region of the catalytic domain, and 495−503 in the C-terminus are missing. Analysis of the model with PROCHECK (*29*) showed that 92.9% of the residues are in most favorable regions and the remaining residues are in additionally allowed regions. Data collection and refinement statistics are summarized in Table 1.

Structure Alignment. We superimposed the Cα atoms of the homologous residues (residues Ser317, Asp358, Gly360, Gly381, Arg382, Tyr405, Glu408, Gly409, and Glu431 for *T. foetus* IMPDH; residues Ser329, Asp364, Gly366, Gly387, Ser388, Tyr411, Met414, Gly415, and Gln441 for hamster IMPDH) with program package O.

Construction, Expression, and Kinetic Characterization of R418A Mutant. The *T. foetus* IMPDH mutant R418A was constructed with site-directed mutagenesis using the QuikChange method (Stratagene, La Jolla, CA). The entire gene was sequenced to ensure no undesired mutation occurred. The R418A mutant was expressed and purified using the methods developed for wild-type enzyme (*30*). IMPDH activity was determined by monitoring the production of NADH by absorbance at 340 nm. Reactions were performed in 100 mM KCl, 50 mM Tris-Cl (pH 8.0), 1 mM DTT, and 3 mM EDTA at 25 °C. MZP is a slow binding inhibitor of IMPDH as previously observed for the human and *E. coli* enzymes (*7, 8*). Progress curves were recorded from reactions, including 24−120 nM MZP, 250 μM IMP, and 800 μM NAD. Enzyme concentrations were 3.6 nM for wild type and 5.0 nM for mutant, respectively. These data are included in Supporting Information. The pre-steady-state experiments were performed on an Applied Photophysics SX.17MV stopped-flow spectrophotometer. The assays contained 2.4 μM enzyme, 0.1 mM IMP and 1 mM NAD.

RESULTS AND DISCUSSION

The E·MZP Complex. MZP is a potent inhibitor of *T. foetus* IMPDH as observed with IMPDHs from other organisms ($K_i = 0.15 \pm 0.05$ nM). To facilitate crystallization, we used a variant of *T. foetus* IMPDH that lacks the

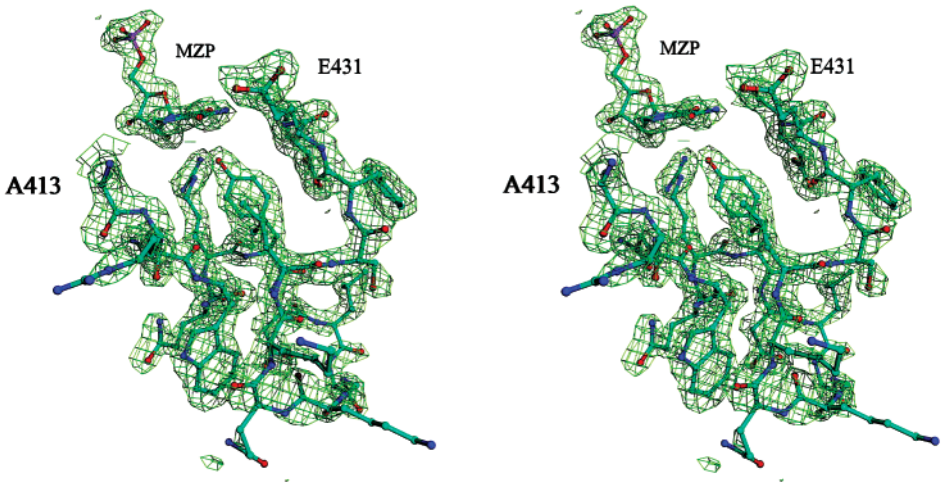

FIGURE 3: Stereoview of the 2Fo-Fc electron density map of the bound MZP and the distal flap. Residues 413−431 are contoured at 1.4σ. Note that the side chains of Arg418 and Tyr419 are in close proximity to the imidazole ring of MZP. C atoms are cyan, O red, and N blue. Wat241 is omitted for clarity.

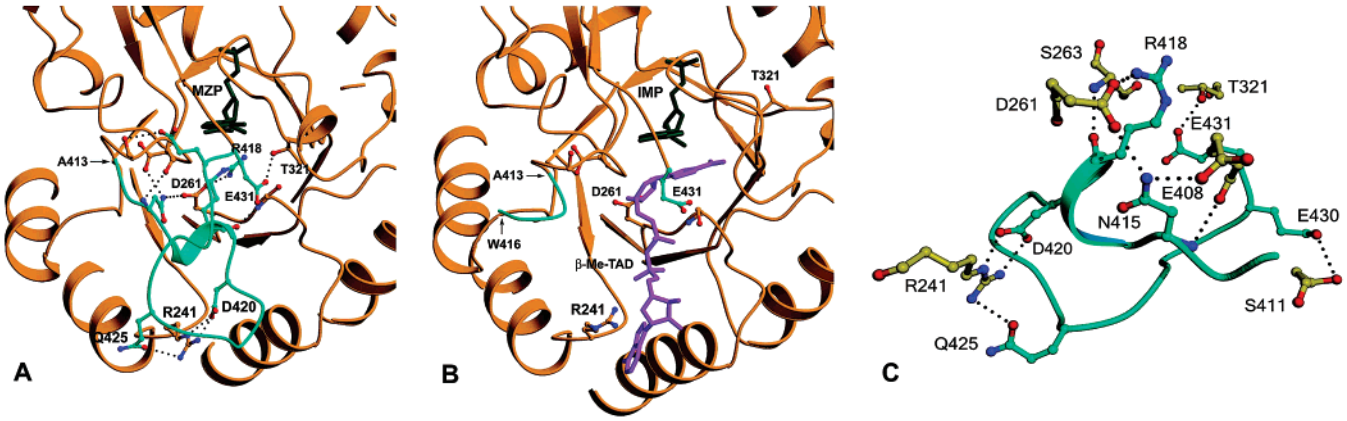

FIGURE 4: The flap binds in the NAD site. (A) The E·MZP complex. (B) The E·IMP·β-Me-TAD complex. (C) The interactions of the flap in the E·MZP complex. The following color scheme is used throughout. IMPDH is orange, the distal flap (residues 413−431) is cyan, MZP and IMP are dark green, and β-Me-TAD is magenta. Where protein side chains are shown, N atoms are blue, and O atoms red. Hydrogen bonds are illustrated as dotted lines. In panel A, residues Ser263, Glu408, Asn415, and Glu430 are not labeled for clarity. This figure was generated with Molscript (*38*) and rendered with Raster3D (*39*).

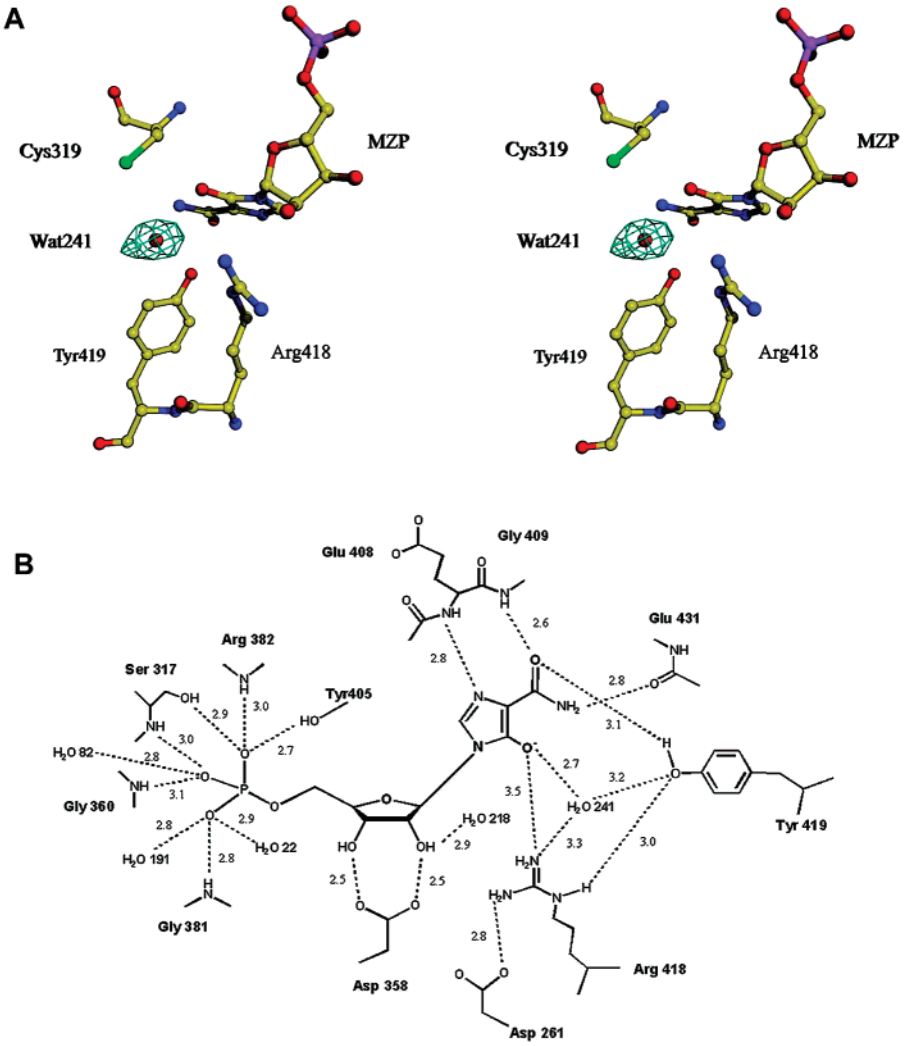

FIGURE 5: The interactions of MZP. (A) The stereoview of the coordination of MZP to Cys319, the Arg−Tyr dyad, and Wat241. Wat241 is poised between the conserved Arg418−Tyr419 dyad. The omit Fo-Fc density map for Wat241 is contoured at 3.0σ. Colors are assigned as follows: C (yellow), N (blue), O (red), S (green), and P (magenta). (B) Schematic representation of the interactions between MZP and IMPDH.

subdomain. Deletion of the subdomain has no effect on the Michaelis−Menten parameters of the enzyme (*15*), nor on MZP inhibition ($K_i = 0.14 \pm 0.04$ nM).

The X-ray crystal structure of the E·MZP complex was solved with molecular replacement methods using the *T. foetus* E·IMP·β-Me-TAD structure as a model (PDB acces-

sion code 1LRT) (*15*). Residues 413−431, which form the distal portion of the active site flap, are largely disordered in the IMPDH structures solved to date, and residues 413−430 were not included in the starting model. As observed in other IMPDH structures, the E·MZP complex is a homotetramer; each monomer is an α/β barrel containing a single active site positioned near the subunit interface (Figure 2). Interestingly, unlike previous structures of *T. foetus* IMPDH (*13*, *15*), no disulfide bond is observed between Cys26 and Cys459, which indicates that this disulfide bond is formed during the crystallization of the other complexes.

Two K^+ ions are observed at each subunit interface. Site 1 is analogous to the K^+ site previously identified in the E-XMP*·MPA complex of hamster IMPDH, but has not been observed in other IMPDH complexes (*12*, *31*). The K^+ at site 1 is coordinated to the main chain carbonyls of active site loop residues Gly314, Gly316, Cys319 and Glu485′, Gly486′ and Gly487′ from the adjacent monomer (the symbol ′ denotes a residue from adjacent monomer). Site 2 has previously been observed in the E·IMP·β-Me-TAD complex of *T. foetus* IMPDH (*15*). The K^+ at site 2 is coordinated to the main chain carbonyls of Gly20, Asn460, and Phe266′, the side chain carboxylate of Asp264′, and the hydroxyl of Ser22.

A Novel Flap Conformation. Unlike previous structures, the entire active site flap is well ordered in the E·MZP complex (Figures 2 and 3). The distal portion of the flap folds into the NAD site, creating a new closed conformation (Figure 4). Residues 416−419 form a short α-helix, with a conserved Arg418−Tyr419 dyad occupying the nicotinamide subsite. Arg241, which stacks against the adenine group of β-Me-TAD, forms hydrogen bonds with Asp420 and Gln425 in the closed conformation. Ser263 and Asp261, which interact with the phosphate and ribose hydroxyls of the tiazofurin portion of β-Me-TAD respectively, form a hydrogen bonding network involving Asn415, Arg418, and Glu408 in the closed conformation (Figure 4). Residues 422−424, which are disordered in other complexes, are in close contact with helix α8 (residues 442−462) and a proline turn (residues 26 to 29) of the N-terminal loop from the adjacent monomer in the E·MZP complex. Interestingly, the last two residues visible in the distal flap of the E·IMP·β-Me-TAD complex, Asn415 and Trp416, have a helical conformation similar to their structure in E·MZP (Figure 4) (*15*). This observation suggests that the distal flap maintains a helical structure and swings in and out of the NAD site like a door on a hinge.

The Transition State Analogy of E·MZP. MZP is clearly identified in the difference electron density map with coefficient $2F_o-F_c$, binding in the IMP site as expected for a competitive inhibitor (Figure 5). Like IMP and E-XMP*, MZP forms hydrogen bonds with Ser317, Asp358, Gly360, Gly381, Arg382, Tyr405, Glu408, Gly409, and Glu431. In addition, MZP forms a new hydrogen bonding network that resembles the transition state for the hydrolysis of E-XMP*. Cys319 is in the plane of the imidazole ring, while Wat241 is poised below the plane, so that the positions of Cys319 and Wat241 mimic the leaving group and attacking water in the hydrolysis of E-XMP*. Wat241 forms hydrogen bonds to both Arg418 and Tyr419, which suggests that this conserved Arg−Tyr dyad activates water. Arg418 also forms hydrogen bonds with Asp261, Tyr419, and O5 of MZP, while

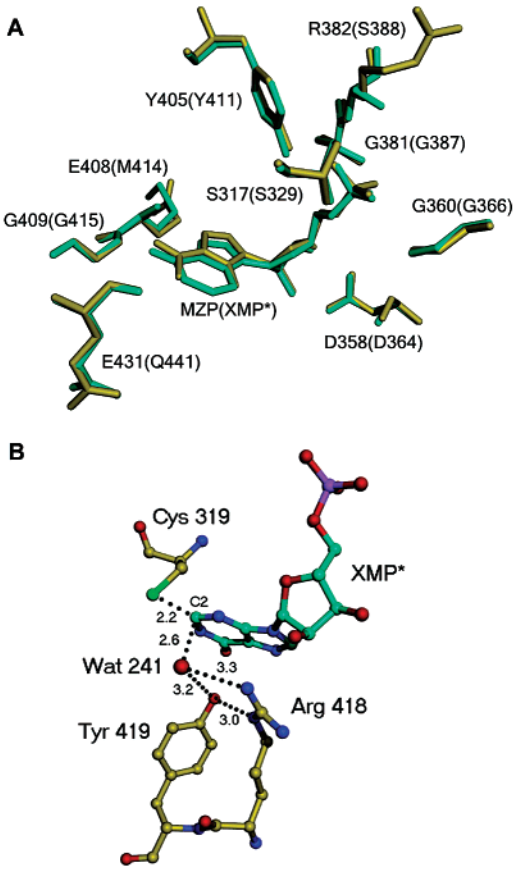

FIGURE 6: The transition state analogy of E·MZP. (A) Superimposition of the *T. foetus* E·MZP structure (yellow) and the hamster E-XMP*·MPA structure (cyan). The hamster numbering is shown in parentheses. (B) Potential interactions of E-XMP* in the closed conformation. Wat241 is positioned for nucleophilic attack of the 2 position of E-XMP*. The distances are indicated with dotted lines. Cys331 covalently linked to XMP* has been omitted for clarity. Colors are assigned as follows: N (blue), O (red), S (green), P (magenta), and C (cyan in XMP* and yellow in residues).

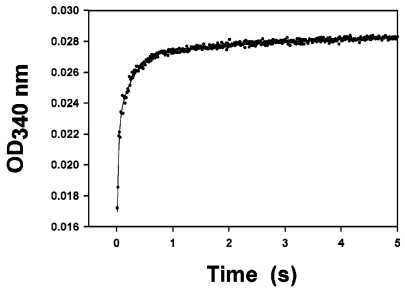

FIGURE 7: The role of the distal flap and Arg418−Tyr419 dyad in the IMPDH reaction. The pre-steady-state reaction of R418A**.** The assay contained 2.4 μM enzyme, 0.1 mM IMP, and 1 mM NAD. The conditions were described in Experimental Procedures.

Tyr419 makes an additional hydrogen bond to the carboxamide oxygen of MZP.

We compared the E·MZP structure with the E-XMP*·MPA complex of hamster IMPDH in order to assess if the closed conformation could form in the presence of E-XMP* (*12*). As shown in Figure 6A, the active sites and nucleotides align with RMSD of 0.17 Å. MZP even adopts the same C3′-endo ribosyl ring pucker as XMP*. This alignment shows that E-XMP* fits easily into the closed conformation (Figure 6B). Hydrogen bonds can form between E-XMP* and both Arg418 and Tyr419, and Wat241 is in position to attack the

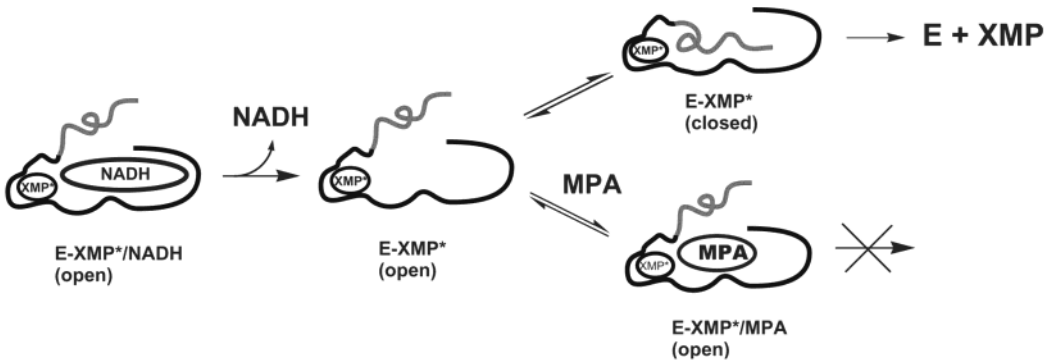

FIGURE 8: A model for the IMPDH reaction. NADH is released, leaving E-XMP* in an open conformation. MPA and the distal flap (in gray) compete for the NADH site. When the closed conformation forms, E-XMP* is hydrolyzed.

C2 atom of E-XMP*. The thiolate of Cys319 is 2.2 Å from the C2 atom of E-XMP*, as might be expected of the leaving group during the hydrolysis reaction. These observations further confirm the transition state analogy of the E·MZP complex.

The Mechanism of Water Activation. The E·MZP structure suggests that the Arg418−Tyr419 dyad activates water for the hydrolysis of E-XMP*. Although the sequence of the distal flap varies greatly among IMPDHs from different sources, the Arg−Tyr dyad is strictly conserved, as expected for crucial catalytic residues (*32*). Substitution of the analogous conserved Arg with Ala inactivates IMPDH from *Streptococcus pyogenes*, confirming that the Arg−Tyr dyad has an important catalytic function (*18*). We constructed the R418A mutant of *T. foetus* IMPDH. As observed in *S. pyogenes* IMPDH, this mutation decreases activity by 400-fold. However, a burst of NADH production equal to 1 NADH/monomer is observed in the pre-steady state, indicating that the rate of NADH production in the first turnover is not affected by the mutation (Figure 7). Hydride transfer is complete within 500 ms, similar to the wild-type enzyme (burst complete within 100 ms (*30*)). Thus, the substitution of Arg418 does not affect the oxidation of IMP to E-XMP* but must specifically impair the hydrolysis of E-XMP*. This observation indicates that the closed conformation is required for the hydrolysis reaction and provides further evidence that the Arg418−Tyr419 dyad activates water.

Implications for Drug Selectivity. MPA is a potent inhibitor of mammalian IMPDHs but a poor inhibitor of microbial enzymes (Figure 1B) (*10*). This selectivity arises partly from differences in the structure of the nicotinamide subsite (*33*), and partly from a previously uncharacterized conformational change of the NAD site (*34*). MPA binds in the nicotinamide end of the NAD site and traps the E-XMP* intermediate (*12*, *35*, *36*) and thus MPA competes with the flap for the NAD site. Intriguingly, MPA resistant IMPDHs generally have higher values of k_{cat} than sensitive enzymes, suggesting that an underlying mechanistic link exists between drug selectivity and catalysis.

The new closed flap conformation provides a structural mechanism linking catalysis with drug selectivity (Figure 8). The enzyme assumes an open conformation for the dehydrogenase phase of the IMPDH reaction. NADH is released, and the flap must move into the NAD site for hydrolysis to occur. The higher the affinity of the flap for the NADH site, the weaker MPA will bind. Thus, the closed flap conformation is the missing conformational change that accounts for MPA selectivity. The more the closed conformation is favored, the faster E-XMP* will be hydrolyzed and, since the hydrolysis of E-XMP* is rate-limiting, the higher the value of k_{cat} will be. This explains why MPA resistant IMPDHs also have higher values of k_{cat} and accounts for the properties of *T. foetus* IMPDH. Conversely, the lower the affinity of the flap for the NADH site, the higher the affinity of MPA and the lower the value of k_{cat}. These are the properties of human IMPDH.

SUMMARY

The structure of the E·MZP complex reveals a transition state analogue complex and solves the mechanistic puzzle of the IMPDH reaction. Water is activated by a conserved Arg−Tyr dyad on a motile flap that moves in and out of the NAD site, converting the enzyme from a dehydrogenase (open conformation) to hydrolase (closed). Drugs such as MPA compete with the flap for the NAD site, so that both catalysis and drug selectivity are controlled by the dynamics of the flap movement.

SUPPORTING INFORMATION AVAILABLE

The progress curves and data fitting used to determine the value of K_i for the inhibition of *T. foetus* IMPDH by MZP. This material is available free of charge via the Internet at http://pubs.acs.org.

REFERENCES

1. Weber, G., Prajda, N., and Jackson, R. C. (1976) *Adv. Enzyme Regul. 14*, 3−24.
2. Allison, A. C. and Eugui, E. M. (1993) *Immunol. Rev. 136*, 5−28.
3. Weber, G. (1983) *Clin. Biochem. 16*, 57−63.
4. Robins, R. K., Revankar, G. R., McKernan, P. A., Murray, B. K., Kirsi, J. J., and North, J. A. (1985) *Adv. Enzyme Regul. 24*, 29−43.
5. Franchetti, P. and Grifantini, M. (1999) *Curr. Med. Chem. 6*, 599−614.
6. Ishikawa, H. (1999) *Curr. Med. Chem. 6*, 575−597.
7. Hager, P. W., Collart, F. R., Huberman, E., and Mitchell, B. S. (1995) *Biochem. Pharmacol. 49*, 1323−1329.
8. Kerr, K. M. and Hedstrom, L. (1997) *Biochemistry 36*, 13365−13373.
9. Wolfenden, R. (1976) *Annu. Rev. Biophys. Bioeng. 5*, 271−306.

10. Hedstrom, L. (1999) *Curr. Med. Chem. 6*, 545−560.
11. Wang, W. and Hedstrom, L. (1997) *Biochemistry 36*, 8479−8483.
12. Sintchak, M. D., Fleming, M. A., Futer, O., Raybuck, S. A., Chambers, S. P., Caron, P. R., Murcko, M. A., and Wilson, K. P. (1996) *Cell 85*, 921−930.
13. Whitby, F. G., Luecke, H., Kuhn, P., Somoza, J. R., Huete-Perez, J. A., Phillips, J. D., Hill, C. P., Fletterick, R. J., and Wang, C. C. (1997) *Biochemistry 36*, 10666−10674.
14. Nimmesgern, E., Black, J., Futer, O., Fulghum, J. R., Chambers, S. P., Brummel, C. L., Raybuck, S. A., and Sintchak, M. D. (1999) *Protein Expr. Purif. 17*, 282−289.
15. Gan, L., Petsko, G. A., and Hedstrom, L. (2002) *Biochemistry 41*, 13309−13317.
16. Goldstein, B. M. and Colby, T. D. (1999) *Curr. Med. Chem. 6*, 519−536.
17. Colby, T. D., Vanderveen, K., Strickler, M. D., Markham, G. D., and Goldstein, B. M. (1999) *Proc. Natl. Acad. Sci. U.S.A. 96*, 3531−3536.
18. Zhang, R., Evans, G., Rotella, F. J., Westbrook, E. M., Beno, D., Huberman, E., Joachimiak, A., and Collart, F. R. (1999) *Biochemistry 38*, 4691−4700.
19. McMillan, F. M., Cahoon, M., White, A., Hedstrom, L., Petsko, G. A., and Ringe, D. (2000) *Biochemistry 39*, 4533−4542.
20. Heyde, E., Nagabhushanam, A., Vonarx, M., and Morrison, J. F. (1976) *Biochim. Biophys. Acta 429*, 645−660.
21. Xiang, B., Taylor, J. C., and Markham, G. D. (1996) *J. Biol. Chem. 271*, 1435−1440.
22. Kerr, K. M., Cahoon, M., Bosco, D. A., and Hedstrom, L. (2000) *Arch. Biochem. Biophys. 375*, 131−137.
23. Sintchak, M. D. and Nimmesgern, E. (2000) *Immunopharmacology 47*, 163−184.
24. Shuto, S., Haramuishi, K., Fukuoka, M., and Matsuda, A. (2000) *J. Chem. Soc., Perkin Trans. 1*, 3603−3609.
25. Otwinowski, A. (1993) Oscillation Data Reduction Program, in Data Reduction and Processing, Proceedings of the CCP4 Study Weekend, 29-30, January, 1993, (Sawyer, L., Isaacs, N., and Bailey, S., Eds.) pp 56−62, SERC Daresbury Laboratory, Warrington, England.
26. Navaza, J. (1994) *Acta Crystallogr., Sect. D: Biol. Crystallogr. 50*, 157−163.
27. Brunger, A. T., Adams, P. D., Clore, G. M., DeLano, W. L., Gros, P., Grosse-Kunstleve, R. W., Jiang, J. S., Kuszewski, J., Nilges, M., Pannu, N. S., Read, R. J., Rice, L. M., Simonson, T., and Warren, G. L. (1998) *Acta Crystallogr., Sect. D: Biol. Crystallogr. 54* (Part 5), 905−921.
28. Jones, T. A., Zou, J. Y., Cowan, S. W., and Kjeldgaard (1991) *Acta Crystallogr., Sect. A 47* (Part 2), 110−119.
29. Laskowski, R. J., MacArthur, M. W., Moss, D. S., and Thorton, J. M. (1993) *J. Appl. Crystallogr. 26*, 283−290.
30. Digits, J. A. and Hedstrom, L. (1999) *Biochemistry 38*, 2295−2306.
31. Futer, O., Sintchak, M. D., Caron, P. R., Nimmesgern, E., DeCenzo, M. T., Livingston, D. J., and Raybuck, S. A. (2002) *Biochim. Biophys. Acta 1594*, 27−39.
32. Zhang, R., Evans, G., Rotella, F., Westbrook, E., Huberman, E., Joachimiak, A., and Collart, F. R. (1999) *Curr. Med. Chem. 6*, 537−543.
33. Digits, J. A. and Hedstrom, L. (1999) *Biochemistry 38*, 15388−15397.
34. Digits, J. A. and Hedstrom, L. (2000) *Biochemistry 39*, 1771−1777.
35. Hedstrom, L. and Wang, C. C. (1990) *Biochemistry 29*, 849−854.
36. Link, J. O. and Straub, K. (1996) *J. Am. Chem. Soc 118*, 2091−2092.
37. Yoshioka, H., Nakatsu, K., Hayashi, M., and Mizuno, K. (1975) *Tetrahedron Lett. 46*, 4031−4034.
38. Kraulis, P. J. (1991) *J. Appl. Crystallogr. 24*, 946−950.
39. Merritt, E. A. and Bacon, D. J. (1997) *Methods Enzymol. 277*, 505−524.

BI0271401